Journal of Materials Chemistry A

ROYAL SOCIETY OF CHEMISTRY

PAPER

View Article Online
View Journal

Cite this: DOI: 10.1039/d5ta10483a

Adsorption kinetics of small molecules on FePt metallic electrodes by classical molecular dynamics simulation

Fan Meng, *[a] Jialong Liu, [b] Qiqi Mo[b] and Noriyoshi Arai [a]

Received 25th December 2025
Accepted 10th April 2026

DOI: 10.1039/d5ta10483a

rsc.li/materials-a

Understanding how long reactants remain on catalytic surfaces (adsorption time) is essential for linking interfacial dynamics to overall reaction efficiency. In complex multistep systems such as the methanol oxidation reaction (MOR), the reaction pathways and surface poisoning are strongly related to the adsorption time and molecule orientation. By employing the molecular dynamics (MD) simulation method, the methanol, sulfuric acid and water molecules on the FePt alloy exposed to (001), (100) and (111) crystal planes were studied, thereby quantitatively defining and evaluating the adsorption time. Methanol exhibits the longest adsorption time, followed by sulfuric acid and water. Molecular conformation analysis further reveals two distinct interfacial regions: a 5 Å guiding layer, where methanol molecules initially approach the surface in a C-down configuration, and a 3 Å reaction layer, where the C–O bonds reorient parallel to the surface. Facet-dependent analysis indicates that the (111) surface, with alternating Pt and Fe atoms, possesses the strongest adsorption capacity, where the adsorption time for methanol is about 18 ps longer compared to the (001) facet. These findings establish a unified framework that quantitatively connects atomic structure, adsorption time, and molecular orientation, which provides a time-resolved perspective for the rational design of FePt-based electrocatalysts.

Introduction

Among various sustainable energy technologies, direct methanol fuel cells have received extensive attention owing to their high energy efficiency, environmental impact, and efficient portability.[1] Clarifying the mechanism of complex electrochemical reactions has always been a challenge to improve the electrocatalytic performance.

Over the past two decades, first-principles calculations have played a pivotal role in electrochemistry, providing fundamental insights towards the design principles of novel nanomaterials for energy devices such as fuel cells and lithium-ion batteries. A representative example is the seminal work by Nørskov and co-workers, who in 2004 calculated the free-energy landscape of the oxygen reduction reaction (ORR) on Pt surfaces and identified the potential-determining step.[2] This thermodynamic approach, based on density functional theory (DFT), excels at predicting thermodynamically stable adsorption configurations and elucidating interfacial reaction mechanisms, thus guiding the experimental catalyst development by enabling rapid screening of overpotentials. Zhou *et al.* computed the most stable adsorption configurations of single volatile organic compound molecules on various metal oxide surfaces,[3] while Li *et al.* revealed that electron localization governs hydrogen adsorption and hydride layer formation on Mg(0001) surfaces.[4] However, the method inherently focuses on reaction energetics at equilibrium and does not explicitly address kinetic effects such as transition-state barriers. In reality, electrode processes are strongly influenced by interfacial phenomena, including double-layer charging, local electric fields, and solvent-mediated proton transfer, all of which can alter kinetics substantially.[5–7] Experimental techniques such as *in situ* infrared spectroscopy and surface-enhanced Raman scattering have successfully identified adsorbed species on catalyst surfaces. But, these methods inherently average over surface aggregation and time scales, obscuring the transient adsorption/desorption dynamics at individual active sites.

Another method, classical molecular dynamics (MD), is emerging as an important supplementary way to simulate the dynamic process in the actual reaction. MD simulations can calculate interfacial processes involving multiple molecules and thousands of atoms, providing a realistic statistical representation of the catalytic environment. Moreover, MD resolves atomic trajectories on the picosecond timescale, enabling direct observation of adsorption, diffusion, and desorption events. These features make MD a powerful tool for investigating kinetic phenomena that govern surface reactions. True electrochemical interfaces are characterized by the presence of an interfacial electric field and a solution phase. Furthermore, differences in electrode surface charge directly lead to changes

[a]Department of Mechanical Engineering, Keio University, Japan. E-mail: mengfan@keio.jp
[b]Department of Physics and Electronics, School of Mathematics and Physics, Beijing University of Chemical Technology, China

in the electrochemical bilayer structure, which brings about changes in reaction kinetics as well as a variety of other possibilities. The presence of the solution phase, on the other hand, promotes proton transfer and lowers the reaction energy barrier. The femtosecond precision makes MD simulations powerful to investigate the kinetic behavior. For example, mean square displacement (MSD) analysis, diffusion coefficient (D), and radial distribution functions (RDFs, $g(r)$) have been widely used to characterize molecular mobility and structural ordering near surfaces.[8–11] The time scales of adsorption behavior of reactants, particularly their adsorption time (τ_{ads}) at active sites, emerge as a critical yet underexplored kinetic determinant. This time dimension dictates whether intermediate species can undergo complete transformation or desorb prematurely, ultimately controlling reaction selectivity and efficiency.[12,13]

Prior studies indicate that methanol, sulfate/sulfuric acid species, and water play distinct interfacial roles and exhibit different adsorption strengths on Pt-based electrodes; however, their time-resolved adsorption behavior has not been quantitatively established. Surface structure can significantly influence the adsorption/desorption thermal dynamics, leading to various adsorption behaviours of different molecular species.[14,15] However, a direct, time-resolved description of adsorption events is not acquired at the molecular level. This gap motivates our analysis of adsorption time distributions across species and facets, which are quite important to explore the complex multistep reactions such as the MOR.

In this work, all-atom classical molecular dynamics simulations are employed to elucidate the relationship between the electrode surface structure and the adsorption behavior of methanol on FePt electrocatalysts with different facets. The adsorption time, a quantitative descriptor, is quantitatively determined, which can provide an intuitive, time-resolved perspective on small-molecule adsorption at catalytic interfaces. Furthermore, the posture configurations of molecules near the surface are analyzed. The study of dynamic processes with MD simulation offers new insights into the molecular-level dynamics of the MOR and helps design Pt-based nanomaterials with specific microstructures.

Method

Simulation model

Simulations were performed with the GROMACS package.[16] The experimental electrolyte used in the reference study consisted of 0.5 M H_2SO_4 and 1 M CH_3OH.[17] Based on the experimental data, the methanol-to-sulfuric acid ratio was set to 2 : 1. To maintain a manageable computational cost, the number of water molecules was moderately reduced. The liquid phase box comprises 2000 methanol molecules, 1000 sulfuric acid molecules, and 30 000 water molecules. After appropriately reducing the number of water molecules, the final concentration of methanol was approximately 1.8–2 mol L^{-1}, and the ratio of methanol to sulfuric acid was 1 : 2. The lateral dimensions of the simulation box (x and y) were fixed at approximately 13 nm to match the electrode slab size. The box length along the z-direction was then determined from the experimental density and the total number of molecules in the system. Water was represented by the TIP4P model, and all intermolecular interactions were described using the General AMBER Force Field version 2 (GAFF2).[18] The force-field combination adopted here has been evaluated in previous studies against solvation and cross-solvation free energies in aqueous and organic environments, providing prior support for its applicability in the present simulations.[19,20] The FePt electrode atoms were modeled using Lennard-Jones parameters derived from the Universal Force Field (UFF).[21] The Lennard-Jones parameters used in the simulations correspond to the values implemented in the GROMACS topology. Cross interactions between different atom types were calculated using the Lorentz–Berthelot combining rules:

$$\sigma_{ij} = \frac{\sigma_i + \sigma_j}{2} \quad (1)$$

$$\varepsilon_{ij} = \sqrt{\varepsilon_i \varepsilon_j} \quad (2)$$

where σ_{ij} and ε_{ij} are the Lennard-Jones size and energy parameters between atom types i and j, respectively.

After energy minimization and equilibration, production runs were conducted in the *NVT* ensemble at 298 K with a time step of 1 fs. The temperature was controlled using the V-rescale thermostat, and atomic charges were assigned with the Gasteiger method.[22] Long-range electrostatic interactions were treated using the particle mesh Ewald (PME) method, while short-range electrostatic and van der Waals interactions were truncated at 1.13 nm. All bonds involving hydrogen atoms were constrained using the LINCS algorithm. For each system, five consecutive *NVT* simulations were performed, each lasting 10 ns, giving a total simulation time of at least 50 ns. The trajectory from the final 10 ns run was used for analysis. The trajectory from the final 10 ns was used for analysis. The molecular trajectories were analyzed and visualized with the OVITO software[23] (Fig. 1).

The lattice parameters of the FePt surface alloy were obtained from the Materials Project database (MP-1198813),[24,25] as listed in Table 1. The surface orientations were constructed based on the $L1_0$-phase structure (JCPDS 43-1358).[26] Three slab models exposing the (100), (001), and (111) surfaces were constructed for the simulations. The atomic coordinates of the FePt electrode slabs were generated using an in-house code based on the crystallographic lattice parameters and surface orientations described above. For the (001) and (100) facets of FePt, the topmost atomic layer can be terminated by either pure Pt atoms or pure Fe atoms because of the layered $L1_0$ ordering. Consequently, two distinct surface terminations, Pt-terminated and Fe-terminated surfaces, naturally arise for these orientations. In contrast, the (111) surface exposes a mixed Fe–Pt atomic layer, making a single, compositionally mixed termination. Under periodic boundary conditions, the simulation cell forms a surface–liquid–surface arrangement. For the FePt(001) and (100) slabs, this arrangement naturally gives rise to one Pt-terminated interface and one Fe-terminated interface, which are analyzed separately in the following sections. The atoms of the electrode slab were kept fixed during the simulations.

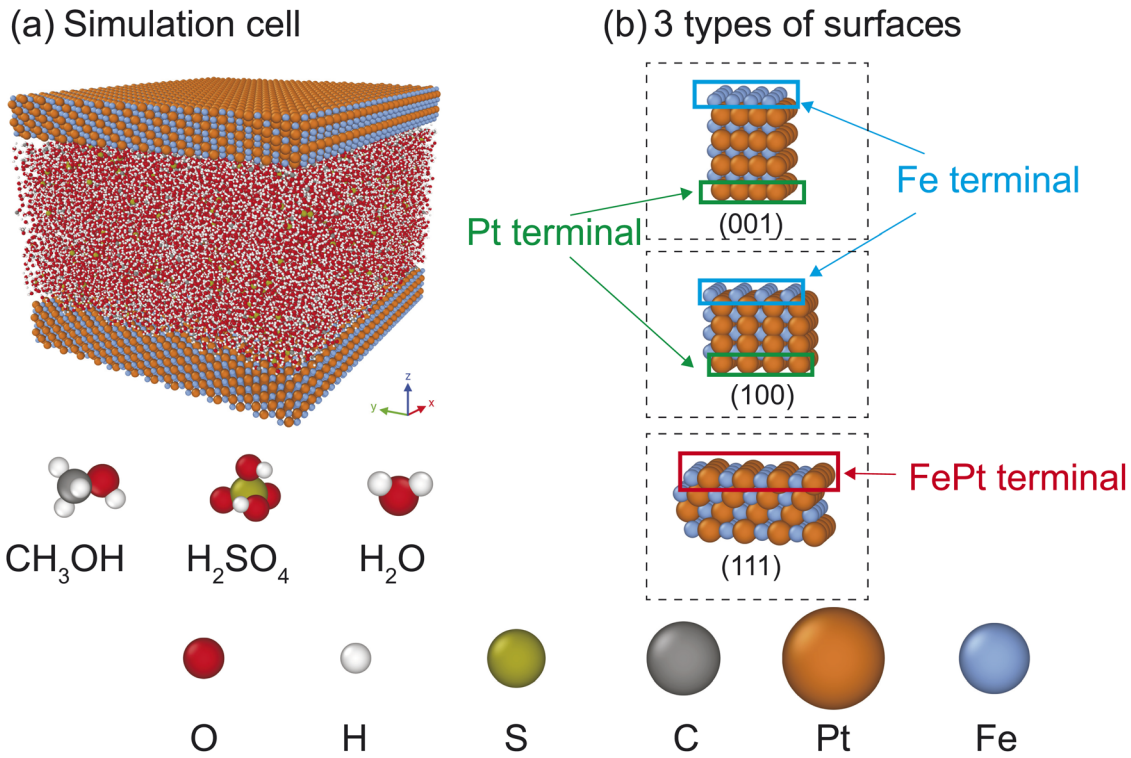

Fig. 1 (a) Molecular dynamics simulation box of the FePt electrode–electrolyte interface. The FePt slab is placed at the bottom of the simulation box and exposed to a mixed electrolyte containing methanol (CH_3OH), sulfuric acid (H_2SO_4), and water (H_2O). Periodic boundary conditions are applied in all directions. (b) Surface atomic structures of FePt with different Miller indices. For the (001) and (100) facets, two distinct terminations are present, corresponding to Pt-terminated and Fe-terminated surfaces. In contrast, the (111) facet exposes a mixed Fe–Pt termination. Atom colors: O (red), H (white), S (yellow), C (gray), Pt (orange), and Fe (blue).

Table 1 Lattice parameters of the FePt alloy

Crystal structure	Lattice (conventional)
Lattice constant a	2.73 Å
Lattice constant b	2.73 Å
Lattice constant c	3.74 Å
Angle α	90.00°
Angle β	90.00°
Angle γ	90.00°
Volume	27.81 Å^3

Detailed force-field parameters and atomic charges used in the simulations are provided in the SI Section S1.

Results and discussion

Density distribution analysis

The distribution of molecules near the surface strongly affects the kinetic dynamics in electrocatalysis, which further influences the formation of an electrical double layer. Also, previous studies have found that the electrode area, surface morphology, and atomic arrangement influence the attachment and movement of molecules.[27,28] As shown in Fig. 2, for the Pt-terminal surface on the left, a pronounced methanol peak appears within the first 3.8 Å, confirming strong methanol adsorption. A minor sulfuric acid peak is also present for the Pt-terminal surface. At the Fe interface, the absence of a density peak for sulfuric acid indicates that it does not adsorb and is weakly repelled by Fe sites. Water and methanol overlap within 4.1 Å of the Pt surface. Previous studies have also reported that competitive adsorption occurs on the catalyst surface.[12]

Comparisons across the three different Miller index surfaces reveal no significant differences in the methanol and water density profiles, while the sulfuric acid density is notably lower near the (111) facet. At a distance of 3 Å from the surface, the sulfuric acid density decreases from approximately 145 kg m^{-3} on the (001) surface to 71 kg m^{-3} on the (111) surface, consistent with stronger sublayer Fe involvement and the associated repulsive interaction at this interface.

Fig. 2(d)–(f) shows the density distributions of each species on the Pt-contact surface with different Miller indices. As shown in Fig. 2(d) and (f), the methanol and water density profiles for the three facets indicate that variations in surface orientation have little influence on surface adsorption behavior. Fig. 2(e) reveals that the three terminal layers affect the sulfuric acid density distribution, as sulfuric acid is repelled from Fe sites. The sulfuric acid density decreases with increasing Fe exposure at the surface, indicating that sulfuric acid molecules are repelled by Fe sites. A minor peak appears on the (001) surface, where the subsurface Fe layer lies farther from the surface. In this configuration, the weaker repulsive influence of Fe atoms allows limited sulfuric acid accumulation, resulting in the small

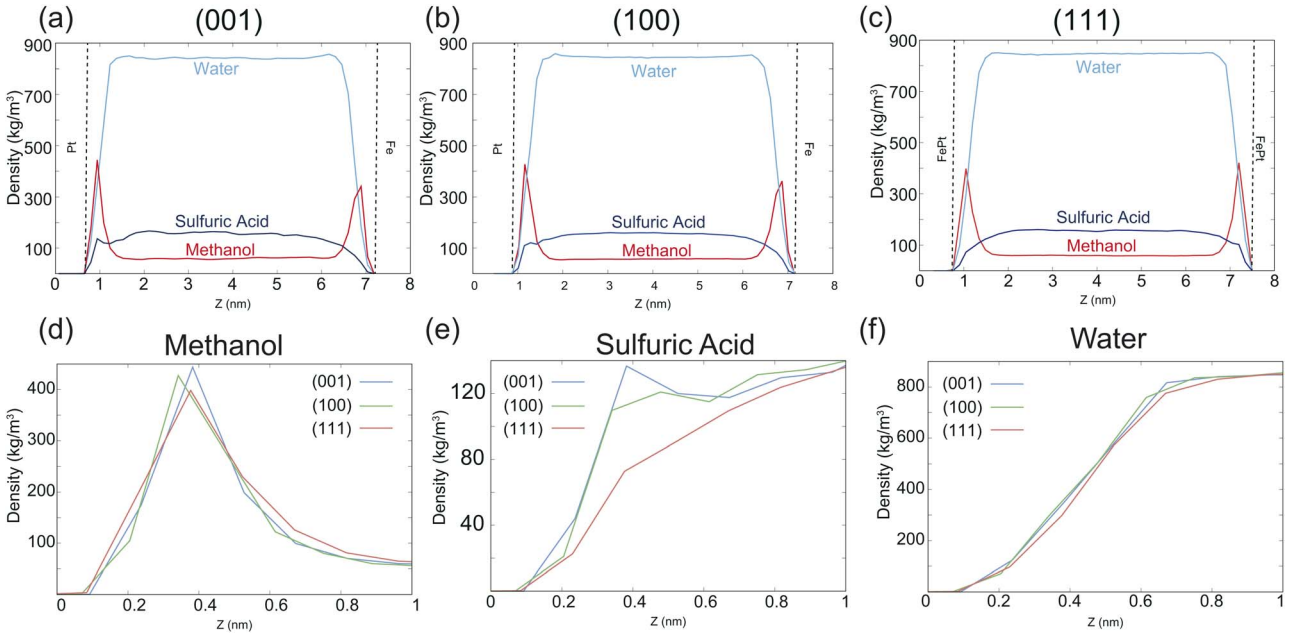

Fig. 2 Density distributions of methanol, sulfuric acid, and water along the axis-*Z* for FePt surfaces with different Miller indices. (a–c) Density profiles across the entire simulation box for the (001), (100), and (111) surfaces, respectively. (d–f) Enlarged density profiles within 1.0 nm from the Pt-contact surface, highlighting the near-surface distributions of methanol, sulfuric acid, and water, respectively, for different surface orientations.

peak observed. The sulfuric acid density on the (100) facet, which exhibits a higher degree of Fe exposure in the subsurface layer, is lower than that on the (001) facet. On the (111) surface, where surface Fe atoms are fully exposed, the sulfuric acid peak vanishes entirely. On the (111) surface, the adsorption of sulfuric acid becomes less favorable, thereby allowing preferential accumulation of methanol and water molecules at the surface.

The density profiles provide valuable information about molecular aggregation near the surface. These analyses offer quantitative insights into interfacial composition, solvation structure, and the thickness of the equilibrium molecular layers, which are highly valuable for guiding experimental studies on surface adsorption and catalyst–electrolyte interactions. However, these static profiles do not directly reflect the time-scale aspect of adsorption. The duration of molecular residence at active sites is particularly important for multistep reactions such as the MOR, where longer adsorption times facilitate more complete reaction pathways. Therefore, the adsorption times of each species were analyzed to obtain a more intuitive, time-resolved understanding of the adsorption behavior.

Adsorption time

The adsorption time of reactants kinetically governs the MOR, and surface poisoning results from an imbalance of reactant adsorption on the catalyst surface.[29–31] Such an imbalance typically results in excessively long adsorption times of CO-producing intermediates or insufficient adsorption of OH-supplying species, leading to incomplete oxidation pathways. In other words, surface poisoning can be mitigated either by shortening the adsorption time of poisoning precursors or by extending the adsorption time of species required to remove them. Therefore, adsorption time serves as a key descriptor for understanding MOR kinetics, as prolonged adsorption at the solid–liquid interface facilitates the complete conversion of intermediates such as CO. Through classical molecular dynamics simulations, we established a method to directly quantify the adsorption time. To determine an appropriate adsorption distance, ten methanol molecules were randomly selected from the entire simulation box, and their center-of-mass positions were tracked along the *z*-axis. These trajectories show that adsorption events consistently occur within 1 nm of the catalyst surface, consistent with the density distribution analysis. Therefore, a 1 nm range was adopted as the effective adsorption region. This choice is also physically justified, as van der Waals interactions in the GAFF2 force field are explicitly evaluated only within the Lennard-Jones cutoff of 1.13 nm. Molecules inside 1 nm are thus subject to the dynamical influence of the surface, whereas those farther away experience negligible direct interactions.

To exclude transient collisions-instances where molecules briefly enter the adsorption region and immediately escape, we defined a molecule as "adsorbed" only if it remained within 1 nm of the surface for longer than 5 ps. This criterion ensures that only meaningful adsorption events are included in the analysis. This criterion is determined through a convergence analysis. Smaller distance thresholds (*e.g.*, 3 Å) result in too few adsorption events with residence times exceeding the cutoff, leading to unstable statistics. The distance and time criteria are

therefore gradually increased until the adsorption-time distributions converge, yielding 1 nm and 5 ps as robust thresholds for defining meaningful adsorption events. It should be noted that the 1 nm criterion used in the adsorption-time analysis does not represent direct surface contact in the strict Helmholtz-layer sense, but rather defines a near-surface residence region for kinetic analysis.

The adsorption time distributions of methanol, sulfuric acid, and water molecules are shown in Fig. 3(a)–(c). The adsorption time distributions of methanol, sulfuric acid, and water were fitted using single Gaussian functions of the form

$$g_i(x) = A_i \exp\left[-\frac{(x-\mu_i)^2}{2\sigma_i^2}\right], \quad i = 1, 2, 3 \tag{3}$$

to quantify their average adsorption times and temporal dispersions. The fitted parameters are listed in Table 2. Considering the Pt-terminal surface, first, methanol, as the main reactant, exhibits the longest adsorption times, ensuring sufficient surface contact for reaction progression. Sulfuric acid molecules display middle-range adsorption times. Rather than acting as a direct reactant in the MOR, they primarily serve to maintain an acidic, ion-conductive environment that facilitates charge transport in the electrolyte. In addition, adsorbed sulfate species partially occupy surface sites and modulate the local electronic environment of the catalyst surface, thereby helping to suppress undesired side processes such as excessive CO adsorption and surface oxidation of the metal. Water molecules, in contrast, show the shortest adsorption times, as they must rapidly participate in surface reactions and continuously replenish OH^- ions. This distribution reflects the functional roles of the three species during the MOR and supports the reliability of our simulation model. Notably, this work quantitatively characterizes—for the first time—the adsorption

Table 2 Gaussian fitting parameters (A, μ, and σ) for adsorption time distributions of methanol, sulfuric acid, and water on FePt surfaces

Surface	Molecule	A	μ (ps)	σ (ps)
(001)	Methanol	0.021	45.583	18.064
	Sulfuric acid	0.044	19.710	9.071
	Water	0.144	11.019	2.619
(100)	Methanol	0.016	53.335	24.135
	Sulfuric acid	0.040	20.381	10.251
	Water	0.117	12.787	3.244
(111)	Methanol	0.018	63.453	20.343
	Sulfuric acid	0.051	20.621	7.286
	Water	0.120	13.893	3.135
(111)-CO	CO	0.028	70.426	13.234
	Sulfuric acid	0.138	13.779	2.627
	Water	0.218	8.865	1.760

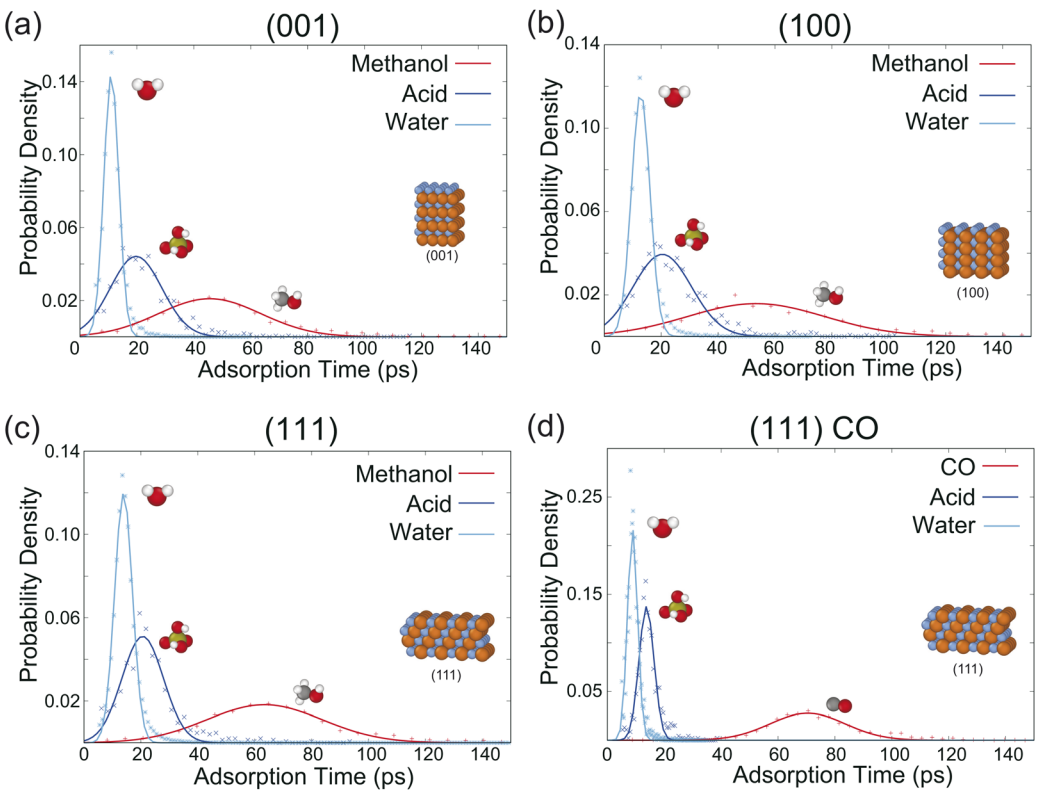

Fig. 3 Probability density distributions of adsorption times for different species on FePt surfaces with different Miller indices. (a–c) Adsorption time distributions of methanol, sulfuric acid, and water on the (001), (100), and (111) surfaces, respectively. Adsorption time is defined as the continuous residence duration of a molecule within 1 nm of the catalyst surface. Solid lines represent Gaussian fits to the probability density distributions. (d) Adsorption time distributions of CO, sulfuric acid, and water on the FePt(111) surface, illustrating the competitive adsorption behavior induced by strong CO binding. The results reveal distinct residence-time hierarchies among different species and highlight the prolonged surface occupation of CO on the (111) facet.

durations of individual reactants in the FePt-catalyzed MOR system, providing an intuitive comparison of how different reactants interact with the surface on distinct time scales.

Facet-dependent adsorption behavior further reveals the structure–function relationship of FePt surfaces. A comparison of the (001) and (100) facets indicates that the average methanol adsorption time on the (100) surface is 7.8 ps longer (Table 2). Previous studies have demonstrated that facet engineering and doping engineering can substantially influence the adsorption behavior of reactants and intermediates, because different crystal planes expose distinct atomic coordination environments, while dopants modify the local geometric structure at the catalyst surface.[14] In our FePt system, the Pt–Pt spacing on the (001) facet is 2.73 Å, while the Pt–Pt spacing on the (111) facet is 3.74 Å. This variation in surface lattice strain enables subsurface Fe atoms to participate more effectively in interfacial interactions with methanol, thereby extending the adsorption time.

In addition to compositional effects, lattice strain in Pt-based catalysts has been reported to modulate the methanol oxidation pathway by tuning the stability of reaction intermediates.[32] Zeng *et al.* have shown that lattice contraction stabilizes formate-related intermediates, while moderate strain enhances CO_2 production through CO intermediates and mitigates CO poisoning.[33] Pt provides stable MOR sites but is susceptible to CO poisoning, and Fe enhances water adsorption and assists in the removal of CO intermediates.[29,34]

Among all facets, the (111) surface shows the most optimal adsorption characteristics. Its alternating Pt–Fe atomic surface arrangement allows Fe to contribute more significantly to adsorption, while Pt serves as the primary catalytic site for the MOR. This configuration integrates the complementary roles of Pt and Fe, with Fe modulating methanol and water adsorption. Notably, methanol adsorption on the (111) surface is 17.9 ps longer than on the (001) surface, highlighting the rationality of FePt as a methanol fuel cell electrode material. The (111) facet maximally leverages the synergistic functions of Fe and Pt, thereby enhancing catalytic performance.

Given the crucial role of CO as a poisoning intermediate in the MOR, we further performed adsorption-time analysis for CO on the FePt(111) surface. As shown in Fig. 3(d), CO exhibits a much longer adsorption duration of 70.4 ps, substantially longer than that of methanol. Such prolonged residence enables CO to occupy active Pt–Fe interfacial sites persistently, thereby blocking methanol adsorption and hindering the overall reaction progress. This finding is consistent with *in situ* spectroscopic observations showing that CO_{ads} can persist on Pt-based surfaces even when conventional electrochemical indicators suggest minimal poisoning, highlighting the importance of resolving adsorption behavior beyond current-based metrics.[35]

In contrast to the methanol-only simulations, where extending methanol residence did not noticeably shorten the adsorption times of sulfuric acid and water, the CO-loaded system shows a distinctly different behavior. In the presence of CO, both sulfuric acid and water display significantly reduced adsorption durations, indicating strong competitive adsorption between CO and these two species. Because sulfuric acid modulates the interfacial ionic environment and water provides hydroxyl radical pathways, the suppression of their adsorption further aggravates MOR deactivation. These results demonstrate that excessively strong CO adsorption not only blocks methanol but also disrupts the adsorption balance of coexisting electrolytes, thereby amplifying CO poisoning effects.

To further understand the interfacial behavior of poisoning intermediates, we additionally analyzed the density distribution of CO along the surface-normal direction (Fig. S1). CO exhibits a pronounced density enhancement near the FePt surface, with a steep increase in the interfacial region of approximately 0.6–0.9 nm from the surface. Compared with methanol under similar conditions, the CO density profile shows a broader interfacial peak, indicating that CO is more strongly localized near the electrode and forms a thicker adsorption layer. In contrast to the methanol-containing system, where methanol and water densities increase more synchronously within about 0.6–1.0 nm, in the CO-containing system H_2SO_4 and H_2O remain relatively low in the 0.6–0.8 nm region and increase more noticeably only at larger distances. These results are consistent with the relatively long adsorption times of CO and support its role in surface poisoning during the MOR process. The growth rate of the CO density profile is substantially higher than that of H_2O, whereas the slope for CH_3OH is comparable to that of H_2O. This suggests that, under the present molecular composition, CH_3OH and H_2O show similar interfacial access and residence behavior, which may be favorable for methanol oxidation at the surface. In contrast, the much steeper increase for CO indicates a stronger tendency for interfacial accumulation, consistent with its slower removal or oxidation at the interface. More detailed density-profile analysis is provided in the SI Section S3.

Generally speaking, the adsorption time distribution obtained in this work is consistent with the mechanistic requirements of the MOR: methanol exhibits the longest adsorption time to ensure sufficient surface residence for oxidation, sulfuric acid maintains the interfacial ionic environment with intermediate-duration adsorption, and water molecules display the shortest adsorption times due to their rapid transport across the interface. Furthermore, our additional analysis of CO reveals that its excessively long adsorption time severely perturbs this balance, displacing both sulfuric acid and water from the surface and thereby amplifying poisoning effects. These findings demonstrate that facet selection and Fe incorporation effectively tune molecular adsorption and interfacial dynamics, providing quantitative guidance for the rational design of FePt-based bifunctional electrocatalysts. Although previous studies have qualitatively suggested differences in adsorption behavior among reactants, the present work provides a quantitative, time-resolved description of these adsorption processes, helping to clarify how individual species interact and compete at the catalytic interface.

Molecular conformation and its role in the MOR

Prior experimental and spectroelectrochemical studies have shown that methanol oxidation on Pt-based surfaces proceeds through multiple surface intermediates, including CO-related

pathways, and that the interfacial molecular environment can significantly influence electrocatalytic behavior.[36–38] While adsorption time analysis establishes how long reactants remain in contact with the surface and validates the time dimension of the MOR pathway, it does not reveal how molecules actually interact with the surface during this adsorption time. To address this complementary aspect, an examination of the contact modes of methanol molecules near the electrode surface is carried out. Two primary configurations were identified: C-down and O-down. In the C-down configuration, the carbon side of methanol approaches the surface first, which may be more conducive to interactions associated with C–H activation. In contrast, the O-down configuration brings the hydroxyl group closer to the surface and may therefore be more favorable for interactions associated with O–H activation.[39] This spatial-orientational perspective, when combined with adsorption lifetime analysis, provides a more complete molecular-level understanding of the reaction mechanism.

To quantitatively describe these orientations, we defined cos θ as the angle between the C–O bond vector of methanol and the positive z-axis perpendicular to the surface. The orientation analysis was carried out for two surface layers with thicknesses of 5 Å and 3 Å (Fig. 4(a) and (b)). These distances were selected with reference to the classical Helmholtz double-layer model that describes the interfacial structure of electrochemical systems. In classical electrochemical interface theory, the electrode–electrolyte boundary is described by an electrical double layer (EDL) composed of the inner Helmholtz plane (IHP) and outer Helmholtz plane (OHP) among others.[40] The IHL is understood to consist of molecules and specifically adsorbed ions in direct contact with the electrode surface, extending on the order of a few Å from the interface.[41] Accordingly, we selected 3 Å as the boundary for the reaction-layer and 5 Å for the guiding-layer analysis in our molecular-dynamics model. The choice of 3 Å approximately corresponds to the molecular dimension of methanol,[42] such that this layer represents the first adsorbed molecular layer in direct contact with the catalyst surface. The 5 Å region was selected to capture the second-layer configurations, which are important for understanding how molecular orientations in the outer layer transform into the first contact layer. Because interfacial molecules are not arranged in perfectly discrete layers but rather in a partially overlapping arrangement, 5 Å provides a more realistic boundary than 6 Å. At 5 Å, most methanol molecules exhibit a C-down orientation. However, closer to the surface, in the 3 Å first contact layer, the cos θ distribution becomes nearly Gaussian, indicating that methanol molecules preferentially lie flat on the surface. Such lying-flat configurations maximize the contact area with the

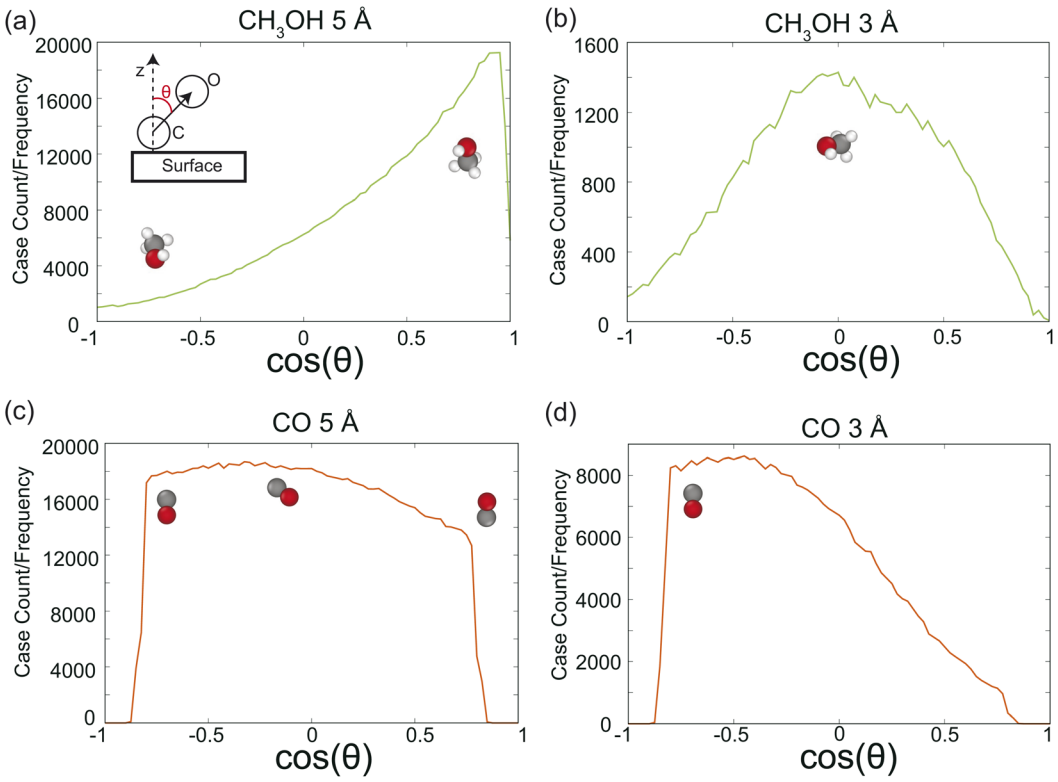

Fig. 4 Orientation distributions of methanol and CO near the FePt(111) surface, expressed as cos θ, where cos θ is the angle between the molecular bond vector and the surface normal. (a and b) cos θ distributions of methanol at distances of 5 Å (guiding layer) and 3 Å (reaction layer) from the surface, respectively. At 5 Å, methanol exhibits a pronounced preference for C-down orientations, whereas at 3 Å the distribution becomes nearly symmetric around cos $\theta = 0$, indicating a surface-parallel configuration. (c and d) cos θ distributions of CO at 5 Å and 3 Å from the surface, respectively. In contrast to methanol, CO predominantly adopts O-down orientations in both layers, suggesting kinetically favored configurations that are less conducive to CO bond activation and oxidation.

surface, representing a pre-reaction state in which both C-down and O-down pathways are accessible. The prevalence of C-down orientations in the 5 Å layer also provides a kinetic explanation for the well-known difficulty in removing CO intermediates during the MOR process.

We define the 5 Å region as a guiding layer, where C atoms act as anchor points due to their stronger interaction with the surface, driving the methanol molecules toward the surface. Upon entering the 3 Å first contact layer, the molecules reorient to a flat configuration, preparing for bond break and subsequent MOR steps. This two-layer adsorption mechanism illustrates how initial C-down attraction facilitates molecular migration, while surface-parallel orientations at the first contact layer enable efficient reaction pathways with minimized CO formation. At this point, the adsorption mechanism diagram of the pre-MOR from a classical molecular dynamics perspective is shown in Fig. 5. The interfacial region above the FePt surface is divided into a reaction layer and a guiding layer. In the guiding layer, reactant molecules are kinetically steered toward the surface, where molecular approach and initial orientation are governed by long-range surface interactions. Upon entering the reaction layer, molecules are in direct contact with surface atoms, adopt surface-parallel configurations, and undergo orientation reorganization that facilitates bond activation and subsequent reaction steps. This two-layer framework provides a unified interpretation of the adsorption-time statistics and orientation distributions observed in the classical molecular dynamics simulations.

We also analyzed the contact configurations of CO at both 5 Å and 3 Å from the surface (Fig. 4(c) and (d)). In contrast to methanol, CO exhibits a dominant O-down orientation in both regions. Because the O atom is more electronegative, O-down contact suppresses electron transfer into the antibonding orbitals of CO, thereby limiting C–O bond activation and hindering its further oxidation. As will be shown in our DFT analysis, CO's C-down configurations are thermodynamically more stable than O-down ones (Fig. 6(f) and (l)). In the C-down geometry, the carbon atom can interact more effectively with the surface through its available lone-pair electrons, thereby facilitating CO activation.

However, our MD results indicate that CO approaches and resides near the surface predominantly in the O-down geometry. This kinetic preference helps explain why CO is difficult to remove during the MOR. Although C-down adsorption would be more favorable for oxidation, the pathway by which CO migrates toward the surface naturally drives it into the less-reactive O-down configuration. If the solution-phase migration pathway could be modulated, such as by applying an external electric field to bias the dipole orientation, CO molecules might arrive at the interface with a higher probability of adopting a C-down configuration, which could significantly enhance CO oxidation efficiency and thereby improve overall MOR performance.

This two-layer adsorption mechanism elucidates how initial C-down attraction facilitates molecular motion, while surface-parallel orientations at the reaction layer enable efficient pathways with minimized CO formation. Moreover, it provides a dynamic perspective that complements classical concepts such as the bifunctional mechanism and d-band theory (thermodynamics). From a catalytic design standpoint, these

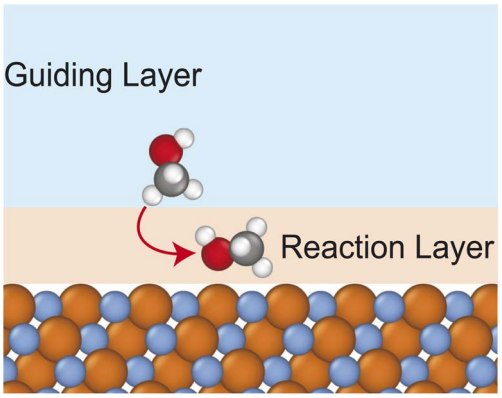

Fig. 5 Schematic illustration of the two-layer interfacial adsorption model.

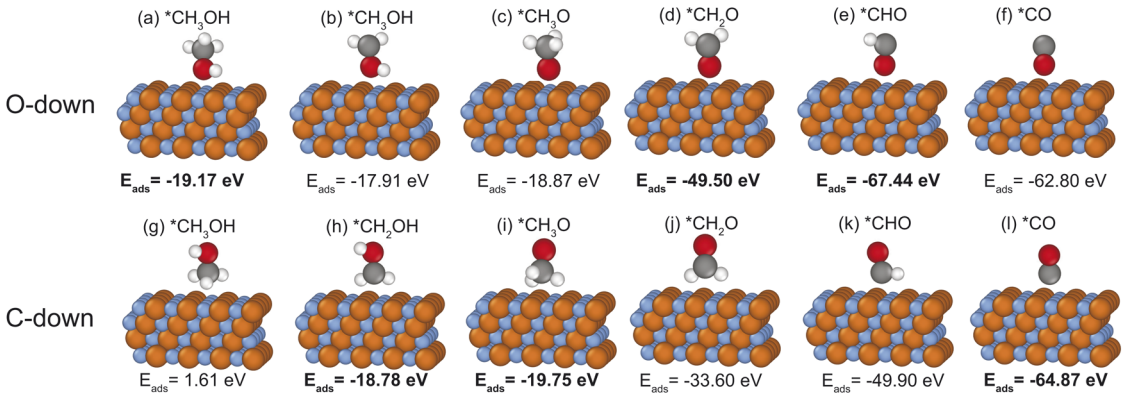

Fig. 6 DFT-optimized adsorption configurations and adsorption energies (E_{ads}) of methanol and key MOR intermediates on the FePt(111) surface. Panels (a–f) show O-down adsorption geometries, while panels (g–l) present the corresponding C-down configurations. The results indicate that both C-down and O-down adsorption modes coexist along the reaction pathway, reflecting the accessibility of multiple adsorption orientations during the MOR.

insights highlight the importance of engineering electrode surfaces that balance strong initial adsorption with facile reorientation, thereby promoting selective MOR pathways while mitigating CO poisoning. Such a molecular-level understanding bridges dynamic simulation results with a thermodynamic perspective and offers guiding principles for the rational design of advanced FePt-based electrocatalysts.

Density functional theory results

To complete the entire reaction process and link kinetics and thermodynamics, DFT calculations were performed to complement the MD simulations and provide energetic validation of the observed adsorption configurations. The theoretical calculations were carried out using Density Functional Theory (DFT) with the generalized gradient approximation (GGA) and the Perdew–Burke–Ernzerhof (PBE) exchange–correlation functional in the CASTEP module of Materials Studio. A 2 × 2 FePt(111) slab with the $L1_0$ phase structure was constructed to simulate the multistep methanol oxidation reaction (MOR) process on the FePt surface. Different adsorption configurations of CH_3OH and the reaction intermediates were examined to identify the most stable adsorption sites.

A vacuum layer of 20 Å was introduced to avoid spurious interactions between periodic images along the surface-normal direction. To represent the bulk-like properties of the FePt slab, the bottom two layers were fixed, while the top layer and the adsorbates were fully relaxed. The plane-wave cutoff energy was set to 520 eV, and the Brillouin zone was sampled using a 3 × 3 × 1 Monkhorst–Pack *k*-point mesh. Structure optimization was performed until the total energy convergence criterion reached 10^{-5} eV. All calculations were spin-polarized.

The adsorption free energies of CH_3OH and the reaction intermediates on the FePt slab were calculated according to

$$\Delta E = E_{\text{ads+substrate}} - E_{\text{substrate}} - E_{\text{ads}} \quad (4)$$

where $E_{\text{ads+substrate}}$ and $E_{\text{substrate}}$ are the Gibbs free energies of the slab with and without the adsorbate, respectively, and E_{ads} is the Gibbs free energy of the isolated adsorbate.

The adsorption energy (E_{ads}) of methanol and its key intermediates was determined on the FePt(111) surface, which provides the most thermodynamically stable adsorption among the examined facets. The details are shown in Fig. 6. CH_2OH, CH_3O, and CO species preferentially adopt a C-down orientation at equilibrium, whereas CH_3OH, CH_2O, and CHO species favor O-down adsorption configurations. This trend indicates that both O-down and C-down configurations exist in the methanol oxidation–reduction reaction pathway. Such phenomena indicate that the MOR does not occur solely through C-down or O-down contacts; the configuration of both contacts is crucial. This aligns with our discussion in a previous section, where we observed that within the 3 Å range of the inner Helmholtz layer (reaction layer), methanol molecules tend to lie flat to prepare for triggering the next reaction stage. MD simulations reveal a kinetic sequence in which methanol first adsorbs in a C-down orientation and later lies down to the O-down state within the reaction layer. It should be noted that the MD and DFT calculations describe the system under different modeling frameworks and solvation environments. The MD simulations include explicit solvent dynamics and classical force-field interactions, whereas the DFT calculations capture adsorption energetics at the electronic-structure level under more idealized conditions. Therefore, comparisons between MD-derived orientations and DFT-derived adsorption configurations should be interpreted qualitatively and viewed as complementary insights.

Linking dynamics with thermodynamics results, we propose a two-layer interfacial mechanism. In the 5 Å guiding layer, the molecular approach is kinetically steered by carbon-surface attraction, so methanol predominantly displays a C-down orientation while migrating toward the interface. Upon entering the 3 Å reaction layer, molecules adopt a surface-parallel geometry and reorient into O-down configurations, at which point thermodynamics becomes dominant and bond activation is facilitated. Furthermore, the difficulty in removing the poisoning intermediate CO during the MOR process can also be attributed to the kinetically dominated C-down configuration within the 5 Å guiding layer. This orientation favors C–H activation pathways that inevitably promote CO formation at the surface. We propose that modulating the interfacial electric field to induce a transition of surface-parallel methanol molecules in the 3 Å reaction layer toward an O-down orientation could effectively suppress CO accumulation and facilitate its removal, thereby improving catalytic capacity.

Conclusions

In this work, all-atom classical molecular dynamics simulations were employed to elucidate the dynamic behavior of methanol and co-reactants at FePt electrode surfaces during the MOR. By introducing adsorption time as a quantitative descriptor, we demonstrated that the adsorption times of water, sulfuric acid, and methanol align with their mechanistic roles in the MOR pathway, thereby validating the simulation framework. Furthermore, orientation analysis revealed a two-layer adsorption mechanism in which initial C-down anchoring in the guiding layer drives molecular migration toward the surface, while subsequent reorientation into surface-parallel configurations in the reaction layer enables efficient O-down pathways with minimized CO formation.

These findings establish a time-resolved and orientationally resolved picture of molecular adsorption that complements traditional thermodynamic descriptions provided by density functional theory. The results not only provide molecular-level support for bifunctional and d-band center concepts in FePt catalysis, but also offer general design principles: effective electrocatalysts should balance strong initial attraction with facile reorientation to promote selective reaction pathways while suppressing poisoning intermediates.

Beyond FePt and the MOR, the framework presented here highlights the broader potential of adsorption-time and contact-mode analysis to unravel interfacial dynamics in complex electrochemical systems. Coupling such molecular dynamics approaches with constant-potential DFT and

multiscale models represents a promising direction toward predictive design of next-generation electrocatalysts.

Author contributions

Conceptualization: F. Meng and J. L. Liu. Methodology: F. Meng and N. Arai. Software: F. Meng. Validation: F. Meng and J. L. Liu. Formal analysis: F. Meng, Q. Q. Mo and J. L. Liu. Investigation: F. Meng and Q. Q. Mo. Resources: N. Arai. Data curation: F. Meng and Q. Q. Mo. Writing – original draft: F. Meng. Writing – review and editing: N. Arai and J. L. Liu. Visualization: F. Meng. Supervision: N. Arai. Project administration: N. Arai. Funding acquisition: N. Arai and J. L. Liu.

Conflicts of interest

There are no conflicts to declare.

Data availability

The datasets supporting the findings of this study, including molecular dynamics and density functional theory results, are available from the corresponding author upon reasonable request.

Supplementary information (SI): the MD simulation parameters, the adsorption time analysis method, and the CO density distribution analysis near the FePt surface. See DOI: https://doi.org/10.1039/d5ta10483a.

Acknowledgements

This work was supported by the National Natural Science Foundation of China (no. 52271163) and the Fundamental Research Funds for the Central Universities (no. PY2516).

References

1 P. Phogat, B. Chand, Shreya, R. Jha and S. Singh, Hydrogen and methanol fuel cells: A comprehensive analysis of challenges, advances, and future prospects in clean energy, *Int. J. Hydrogen Energy*, 2025, **109**, 465–485.
2 J. K. Nørskov, J. Rossmeisl, A. Logadottir, L. Lindqvist, J. R. Kitchin, T. Bligaard and H. Jónsson, Origin of the Overpotential for Oxygen Reduction at a Fuel-Cell Cathode, *J. Phys. Chem. B*, 2004, **108**, 17886–17892.
3 K. Zhou, W. Ma, Z. Zeng, X. Ma, X. Xu, Y. Guo, H. Li and L. Li, Experimental and DFT study on the adsorption of VOCs on activated carbon/metal oxides composites, *Chem. Eng. J.*, 2019, **372**, 1122–1133.
4 B. Li, C. Xiao, N. M. Harrison, R. M. Fogarty and A. P. Horsfield, Role of electron localisation in H adsorption and hydride formation in the Mg basal plane under aqueous corrosion: a first-principles study, *Phys. Chem. Chem. Phys.*, 2023, **25**, 5989–6001.
5 P. Li, Y. Jiao, J. Huang and S. Chen, Electric Double Layer Effects in Electrocatalysis: Insights from Ab Initio Simulation and Hierarchical Continuum Modeling, *JACS Au*, 2023, **3**, 2640–2659.
6 G. Shi, T. Lu and L. Zhang, Understanding the interfacial water structure in electrocatalysis, *Natl. Sci. Rev.*, 2024, **11**, nwae241.
7 T. Liu, Q.-X. Chen, Z. He, J.-L. Wang, S.-Z. Sheng, J.-W. Liu and S.-H. Yu, Efficient Methanol Oxidation Kinetics Enabled by an Ordered Heterocatalyst with Dual Electric Fields, *J. Am. Chem. Soc.*, 2025, **147**, 5340–5349.
8 Z. Taheri and A. Nakhaei Pour, Studying of the adsorption and diffusion behaviors of methane on graphene oxide by molecular dynamics simulation, *J. Mol. Model.*, 2021, **27**, 59.
9 H. Zhao, Y. Lyu, J. Hu, M. Li, H. Chen, Y. Jiang, M. Tang, Y. Wu and W. Sun, Reveal the major factors controlling quinolone adsorption on mesoporous carbon: Batch experiment, DFT calculation, MD simulation, and machine learning modeling, *Chem. Eng. J.*, 2023, **463**, 142486.
10 N. Lu, X. Dong, Z. Chen, H. Liu, W. Zheng and B. Zhang, Effect of solvent on the adsorption behavior of asphaltene on silica surface: A molecular dynamic simulation study, *J. Pet. Sci. Eng.*, 2022, **212**, 110212.
11 T. Kinjo, M. Tsuji, T. Kusano, R. Jinnouchi, S. Makino and H. Nakamura, Effect of substitution degree and dissociation on adsorption behavior of carboxymethyl cellulose on graphite surfaces, *Chem. Phys. Lett.*, 2026, **883**, 142514.
12 W. Huang, K. Xu, L. Liang, K. Shi, Y. Zheng, Y. Min, Z. Cui and Q. Liu, Tracking methanol oxidation reaction from OH* as guiding agent, *Chem. Eng. Sci.*, 2024, **292**, 119991.
13 W. Zhang, B. Huang, Y. Cui, L. Shen and S. Yan, Investigation of the mechanism of methanol electrooxidation: a potential-dependent DFT study, *RSC Adv.*, 2025, **15**, 11056–11064.
14 J. Li, F. Yang and L. Feng, Progress of supported Pt-based catalysts for electrochemical methanol energy conversion, *Coord. Chem. Rev.*, 2025, **534**, 216603.
15 R. Yu, Y. Zhang, S. Deng, R. Zhu, S. Zhang, J. Zhang, Y. Zhao and Z. Xia, Platinum Alloys for Methanol Oxidation Electrocatalysis: Reaction Mechanism and Rational Design of Catalysts with Exceptional Activity and Stability, *Catalysts*, 2024, **14**(1), 60.
16 H. Berendsen, D. van der Spoel and R. van Drunen, GROMACS: A message-passing parallel molecular dynamics implementation, *Comput. Phys. Commun.*, 1995, **91**, 43–56.
17 Q. Mo, R. Liu, F. Meng, Y. Juan, J. Li, S. Wang, N. Arai, J. Liu and W. Wang, Phase transition and ternary alloying synergistically boosting magnetic field response for methanol oxidation reaction on $L1_0$-FeCrPt nanochains, *Appl. Catal., B: Environ. Energy*, 2026, **387**, 126475.
18 J. Wang, R. M. Wolf, J. W. Caldwell, P. A. Kollman and D. A. Case, Development and testing of a general Amber force field, *J. Comput. Chem.*, 2004, **25**, 1157–1174.
19 S. Kashefolgheta, S. Wang, W. E. Acree and P. H. Hünenberger, Evaluation of nine condensed-phase force fields of the GROMOS, CHARMM, OPLS, AMBER, and OpenFF families against experimental cross-solvation

free energies, *Phys. Chem. Chem. Phys.*, 2021, **23**, 13055–13074.
20 X. He, V. H. Man, W. Yang, T.-S. Lee and J. Wang, A fast and high-quality charge model for the next generation general AMBER force field, *J. Chem. Phys.*, 2020, **153**, 114502.
21 A. K. Rappe, C. J. Casewit, K. S. Colwell, W. A. I. Goddard and W. M. Skiff, UFF, a full periodic table force field for molecular mechanics and molecular dynamics simulations, *J. Am. Chem. Soc.*, 1992, **114**, 10024–10035.
22 J. Gasteiger and M. Marsili, A new model for calculating atomic charges in molecules, *Tetrahedron Lett.*, 1978, **19**, 3181–3184.
23 A. Stukowski, Visualization and analysis of atomistic simulation data with OVITO-the Open Visualization Tool, *Modell. Simul. Mater. Sci. Eng.*, 2010, **18**, 015012.
24 A. Jain, S. P. Ong, G. Hautier, W. Chen, W. D. Richards, S. Dacek, S. Cholia, D. Gunter, D. Skinner, G. Ceder and K. A. Persson, Commentary: The Materials Project: A materials genome approach to accelerating materials innovation, *APL Mater.*, 2013, **1**, 011002.
25 M. K. Horton, *et al.*, Accelerated data-driven materials science with the Materials Project, *Nat. Mater.*, 2025, **24**, 1522–1532.
26 M. Zhu, Y. Wang, Y. Wu, J. Liu, J. Zhang, H. Huang, X. Zheng, J. Shen, R. Zhao, W. Zhou and S. Wang, Greatly Enhanced Methanol Oxidation Reaction of CoPt Truncated Octahedral Nanoparticles by External Magnetic Fields, *Energy Environ. Mater.*, 2023, **6**, e12403.
27 W. Dai, K. Wan, K. Pang, J. Guo, S. Liu, K. Wu, C. Tang, Y. Sun, X. Shi, Z. Tang, C. Long and F. Dong, In-depth understanding and precise modulation of surface reconstruction during heterogeneous electrocatalysis: From model to practical catalyst, *Chem*, 2025, **11**, 102345.
28 J. Liang, F. Ma, S. Hwang, X. Wang, J. Sokolowski, Q. Li, G. Wu and D. Su, Atomic Arrangement Engineering of Metallic Nanocrystals for Energy-Conversion Electrocatalysis, *Joule*, 2019, **3**, 956–991.
29 J. Wang, B. Zhang, W. Guo, L. Wang, J. Chen, H. Pan and W. Sun, Toward Electrocatalytic Methanol Oxidation Reaction: Longstanding Debates and Emerging Catalysts, *Adv. Mater.*, 2023, **35**, 2211099.
30 S. Dai, M. Li, H. Li, Y. Shi, H. Zhang, D. Wang, K. Xiang, J. Zou and G. Luo, Advancements in Electrocatalytic Methanol Oxidation: Catalyst Design, Reaction Mechanisms, and Renewable Energy Applications, *ChemSusChem*, 2025, **18**, e202402767.
31 Y. Liu, R. Wu, Y. Jin, J. Dong, H. Li and J. Wang, Balancing reactant adsorption for ultra-stable electrocatalytic methanol oxidation reaction, *eScience*, 2025, **5**, 100430.
32 T. He, W. Wang, F. Shi, X. Yang, X. Li, J. Wu, Y. Yin and M. Jin, Mastering the surface strain of platinum catalysts for efficient electrocatalysis, *Nature*, 2021, **598**, 76–81.
33 R. Zeng, Y. Yang, T. Shen, H. Wang, Y. Xiong, J. Zhu, D. Wang and H. D. Abruña, Methanol Oxidation Using Ternary Ordered Intermetallic Electrocatalysts: A DEMS Study, *ACS Catal.*, 2020, **10**, 770–776.
34 Z. W. Seh, J. Kibsgaard, C. F. Dickens, I. Chorkendorff, J. K. Nørskov and T. F. Jaramillo, Combining theory and experiment in electrocatalysis: Insights into materials design, *Science*, 2017, **355**, eaad4998.
35 A. M. Hofstead-Duffy, D.-J. Chen, S.-G. Sun and Y. J. Tong, Origin of the current peak of negative scan in the cyclic voltammetry of methanol electro-oxidation on Pt-based electrocatalysts: a revisit to the current ratio criterion, *J. Mater. Chem.*, 2012, **22**, 5205–5208.
36 A. V. Selivanova, V. G. Demina, E. E. Aydakov, A. A. Saraev, V. V. Kaichev and V. I. Bukhtiyarov, Mechanistic study of methanol oxidation on Pt(111) single crystal, *Appl. Surf. Sci.*, 2022, **579**, 152140.
37 W. Chen, J. Cai, J. Yang, M. M. Sartin and Y.-X. Chen, The kinetics of methanol oxidation at a Pt film electrode, a combined mass and infrared spectroscopic study, *J. Electroanal. Chem.*, 2017, **800**, 89–98.
38 J.-T. Li, Q.-S. Chen and S.-G. Sun, In situ microscope FTIR studies of methanol adsorption and oxidation on an individually addressable array of nanostructured Pt microelectrodes, *Electrochim. Acta*, 2007, **52**, 5725–5732.
39 T. L. M. Pham, D.-V. N. Vo, H. N. T. Nguyen and N.-N. Pham-Tran, CH versus OH bond scission in methanol decomposition on Pt(111): Role of the dispersion interaction, *Appl. Surf. Sci.*, 2019, **481**, 1327–1334.
40 G. Zhang and M. Schreier, Leveraging electrochemical double layer structure to rationally control electrolysis, *Natl. Sci. Rev.*, 2024, **11**, nwae299.
41 A. H. B. Dourado, Electric Double Layer: The Good, the Bad, and the Beauty, *Electrochem*, 2022, **3**, 789–808.
42 X. Zhang, A. Savara and R. B. Getman, A Method for Obtaining Liquid–Solid Adsorption Rates from Molecular Dynamics Simulations: Applied to Methanol on Pt(111) in H_2O, *J. Chem. Theory Comput.*, 2020, **16**, 2680–2691.